Journal of Medicinal Chemistry

Article

An Ursolic Acid-derived Small Molecule Triggers Cancer Cell Death through Hyperstimulation of Macropinocytosis

Lin Sun, Bin Li, Xiaohui Su, Ge Chen, Yaqin Li, Linqian Yu, Li Li, and Wanguo Wei

J. Med. Chem., **Just Accepted Manuscript** • DOI: 10.1021/acs.jmedchem.7b00592 • Publication Date (Web): 05 Jul 2017

ACS Publications

Journal of Medicinal Chemistry is published by the American Chemical Society. 1155 Sixteenth Street N.W., Washington, DC 20036

An Ursolic Acid-derived Small Molecule Triggers Cancer Cell Death through Hyperstimulation of Macropinocytosis

Lin Sun,[†] Bin Li,[†] Xiaohui Su,[†] Ge Chen,[‡] Yaqin Li,[†] Linqian Yu,[†] Li Li,[*§] and Wanguo Wei[*†‡]

[†]Shanghai Advanced Research institute, Chinese Academy of Sciences, University of Chinese Academy of Sciences, 99 Haike Road, Shanghai, 201210, China

[‡]School of Life Science and Technology, ShanghaiTech University, 100 Haike Road, Shanghai, 201210, China

[§]State Key Laboratory of Oncogenes and Related Genes, Renji-Med X Clinical Stem Cell Research Center, Ren Ji Hospital, School of Biomedical Engineering, Shanghai Jiao Tong University, Shanghai 200127, China.

KEYWORDS: Ursolic acid (UA)· Cancer · Cell death · Methuosis · Macropinocytosis

ABSTRACT: Macropinocytosis is a transient endocytosis which internalizes extracellular fluid and particles into vacuoles. Recent studies suggest that hyperstimulation of macropinocytosis can induce a novel non-apoptotic cell death, methuosis. In this report, we describe the identification

of an ursolic acid-derived small molecule (compound **17**), which induces cancer cell death through hyperstimulation of macropinocytosis. **17** causes the accumulation of vacuoles derived from macropinosomes based on transmission electron microscopy, time-lapse microscopy and labeling with extracellular fluid phase tracers. The vacuoles induced by **17** separate from other cytoplasmic compartments, but acquire some characteristics of late endosomes and lysosomes. Inhibiting hyperstimulation of macropinocytosis with the specific inhibitor, amiloride, blocks cell death, implicating that **17** leads to cell death via macropinocytosis, which is coincident with methuosis. Our results uncovered a novel cell death pathway involved in the activity of **17**, which may provide a basis for further development of natural-product-derived scaffolds for drugs that trigger cancer cell death by methuosis.

INTRODUCTION

Resistance of human tumors to cancer chemotherapeutic agents remains a major and unsolved problem in clinical oncology. In general, cancer cells adapt to the microenvironment changed by drugs through decreasing intracellular drug accumulation and altering apoptotic pathways.[1, 2] Apoptosis is taken as a primary therapeutic focus and target for the treatment of cancer.[3] Acquired drug resistance usually occurs in company with genetic and epigenetic changes, such as p53 mutation, methylation of DNA and acetylation of histone.[4, 5] To avoid resistance to pro-apoptotic drugs, strategies have been developed wherein non-apoptotic target is exploited as new therapeutic strategy for sensitization of malignancies.

Various non-apoptotic forms of cell death have been reported.[6, 7] Morphological characteristics are usually used to distinguish between different forms of cell death. Vacuoles in cytoplasm are morphological features existing in several non-apoptotic cell death subroutines, such as autophagic cell death, necroptosis, paraptosis, and oncosis. Methuosis is a newly discovered

form of non-apoptotic cell death phenotype characterized by accumulation of vacuoles derived from macropinosomes and endosomes.[8, 9] Macropinocytosis was usually recognized as a form of endocytosis which usually happened in immune responses, while latest evidences reveal that it is aberrantly activated in methuosis. Presence of large vacuoles in cytoplasm is the most prominent morphological feature of macropinocytosis. As a novel form of non-apoptotic cell death, methuosis has drawn special attention as a new target for cancer therapy, which has been confirmed in cells manipulated genetically or pharmacologically.[10, 11] Therefore, the identification of small molecules that induced methuosis can provide useful probes to study non-apoptotic cell death and may lead to the development of new therapeutic interventions. Herein, we report the identification and preliminary biological characterization of the natural-product-derived small molecule **17**, which induces cancer cell death through hyperstimulation of macropinocytosis.

RESULTS AND DISCUSSION

Chemistry. Triterpenoids are a large and diverse class of natural products widely distributed in the plant kingdom, which exhibit a broad spectrum of pharmacological activities which are under investigations worldwide for various therapeutic properties.[12-14] For example, ursolic acid (3*β*-hydroxyurs-12-en-28-oic acid, UA) is a well-known pentacyclic triterpenoid carboxylic acid obtained from various medicinal herbs and fruits. It has been reported to show significant anticancer activity against different kinds of tumor cell lines.[15-17] However, the limited solubility, low tumor-targeting specificity and poor bio-availability of UA restricts its further clinical application.[18] Recently, there has been a renewed interest in common dietaries and plant-based traditional medicines for the prevention and treatment of cancer. Therefore, structural

modifications of UA have been widely investigated in order to improve its biological activities and bioavailability.[19-21]

In this regard, a series of novel pyrazole-fused ursolic acid derivatives[22-23] were synthesized as shown in Scheme 1. First, UA was treated with benzyl bromide in the presence of K_2CO_3 in DMF to form benzyl ester (**2**) to ensure a higher yield and better purification process. Oxidation of the benzyl ursolate by Jone's reagent afforded 3-oxo-ursolic acid (**3**) in 84% yield. Then, formylation at C2 position was realized using sodium methoxide and ethyl formate to give ketoaldehydes **4a** (R^1 = H). Introduction of methyl carbonyl group was also accomplished using sodium methoxide and ethyl acetate under the same condition to give **4b** ($R^1 = CH_3$). While the installation of trifluoromethyl carbonyl group at C2 position was realized by using Potassium *tert*-butoxide and ethyl trifluoroacetate in THF to form **4c** ($R^1 = CF_3$) in high yield. Subsequently, the installed carbonyl groups reacted smoothly with various hydrazine hydrochlorides ($R^2NHNH_2{\cdot}HCl$) under basic conditions, and the pyrazole moieties were then formed simultaneously to give various pyrazole-fused ursolates with complete region-selectivity. Finally, the benzyl group was facilely removed by catalytic hydrogenation under 1 atm of H_2 to give the corresponding pyrazole-fused ursolic acid derivatives in high yeilds.

Scheme 1. Synthesis of pyrazole-fused ursolic acid derivatives[a]

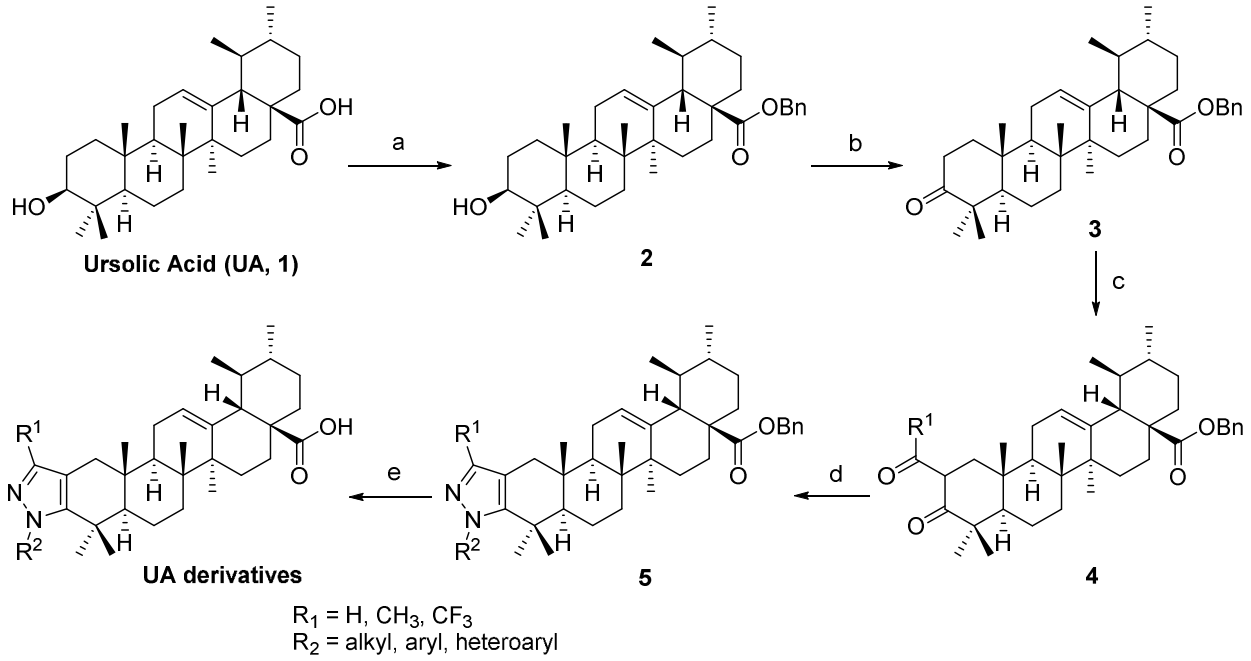

[a]*Reagents and conditions:* (a) BnBr, K_2CO_3, DMF, 60 °C, 92%. (b) PCC, CH_2Cl_2, 0 °C - rt, 84%. (c) R^1CO_2Et (R^1 = H, Me), NaOMe, THF, rt; R^1CO_2Et (R^1 = CF_3), *t*-BuOK, THF, rt, 70%. (d) $R^2NHNH_2 \cdot HCl$, EtOH, rt. (e) H_2, Pd/C, MeOH, rt.

Biological Evaluation. The pyrazole-fused ursolic acid derivatives were evaluated for their *in vitro* anticancer activities against five human cancer cell lines: cervical carcinoma HeLa cells, hepatocelluar carcinoma HepG2 cells, fibrosarcoma HT1080 cells, mammary adenocarcinoma MCF-7 cells, and neuroblastoma SK-N-MC cells. More than 100 compounds (20 μM in DMSO) were evaluated by CCK-8 assay in vitro, and found that most of the pyrazole-fused ursolic acid derivatives also exhibited some inhibitory activities against the five cancer cell lines, and some of them showed much more stronger anti-cancer activities than ursolic acid (UA) in certain cancer cell lines (Table 1). Interestingly, a number of ursolic acid derivatives were found to induce cellular vacuolization that are readily detected by phase-contrast microscopy (see the Supporting Information, Figure S1).

Table 1. Biological evaluation of ursolic acid-derivatives

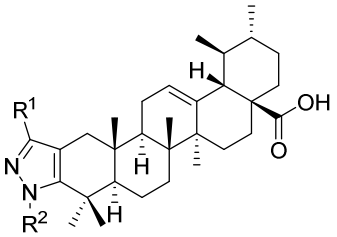

Compd (20 μM)	R^1	R^2	Viability (CCK-8 assay, 48 h)					Vacuole
			HeLa	HepG2	HT1080	MCF-7	SK-N-MC	
UA	–	–	43.30±2.22	34.12±0.68	39.43±0.52	57.64±5.75	67.21±1.78	NO
5	H	CH_3	44.86±2.89	45.97±1.12	35.78±0.33	47.59±0.47	67.44±2.59	YES
6	H		47.05±1.07	56.96±2.02	39.05±0.61	40.53±0.42	63.30±0.25	NO
8	H		30.80±0.42	44.57±0.12	27.88±0.25	36.18±2.38	31.40±1.12	YES
11	H		19.94±1.83	33.85±0.93	23.49±0.40	33.36±2.60	33.89±1.38	NO
12	H		54.20±2.19	56.80±2.00	30.92±2.25	39.69±1.84	79.88±2.36	NO
17	H	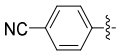	18.63±2.34	27.87±2.98	26.78±0.07	25.25±0.07	28.63±1.03	YES
18	H	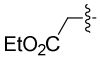	44.16±1.27	43.67±1.25	55.18±1.67	28.91±0.85	66.56±2.07	NO
19	H		40.87±1.44	60.08±2.24	38.70±0.24	46.55±1.67	57.40±1.08	NO
20	H		33.32±1.18	29.49±1.63	33.50±0.37	46.65±1.37	24.61±1.10	NO
21	H	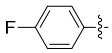	24.39±0.46	58.63±1.92	27.30±0.27	34.29±1.18	39.36±2.36	YES
22	CF_3	CH_3	44.86±2.89	45.97±1.12	35.78±0.33	47.59±0.47	67.44±2.59	YES
23	H	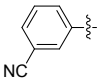	37.33±1.06	29.26±1.87	37.51±1.04	28.14±1.30	30.96±2.11	YES

*Results are expressed as percent of controls that received vehicle alone (DMSO). Values are the mean ± SD.

Of the compounds, **17** was found to significantly suppress cell viability in all tested carcinoma cells, with a quick and striking accumulation of numerous phase-lucent cytoplasmic vacuoles within 12 h (Figure 1B). The effects of **17** on normal human dermal fibroblasts (HDFs) and myoblast cell line (C2C12) were also evaluated, with less vacuoles and reduced cell viability (~13% for C2C12 and 28% for fibroblasts) were observed (Figure 2A, B). Therefore, compound **17** was chosen for further study as a potential inducer of cell vacuolization and death.

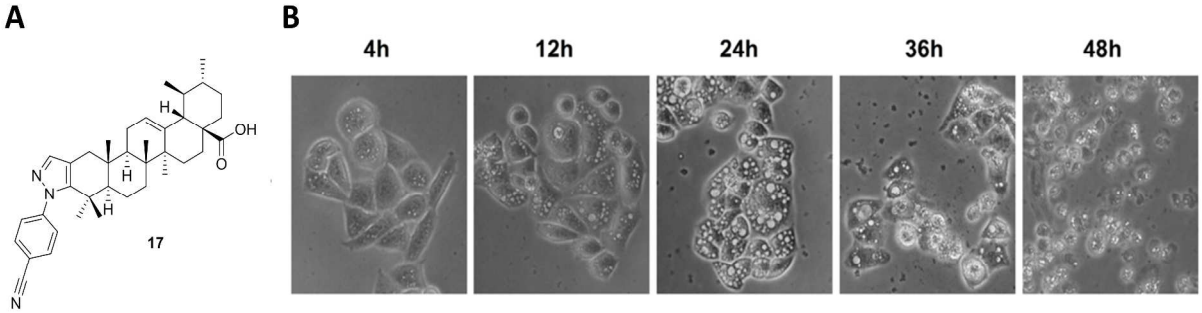

Figure 1. 17 induces cellular vacuolization. (A) The structure of **17**. (B) HeLa cells were treated with **17** at 20 μM, and phase contrast images of live cells were obtained.

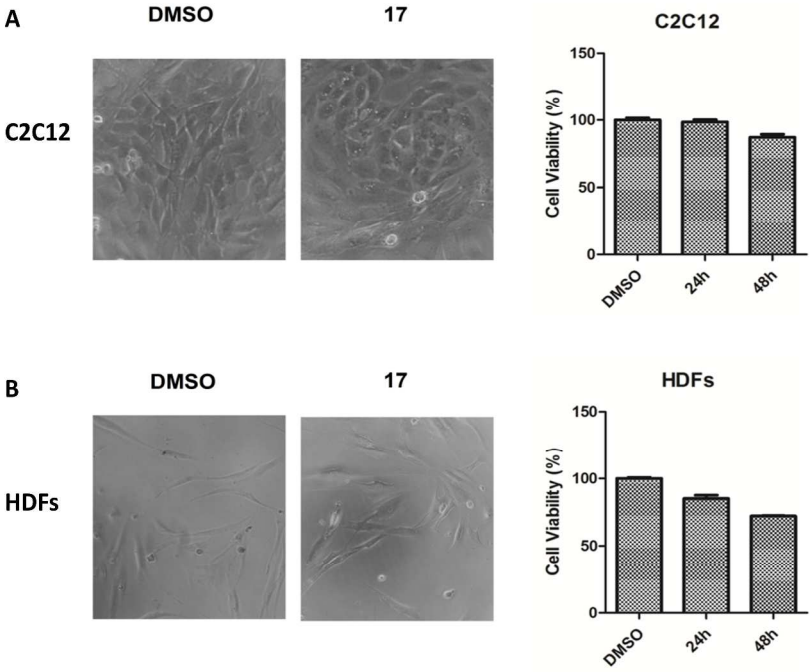

Figure 2. Assay for cytotoxicity in normal cells treated with **17**. (A) Phase-contrast images were obtained after treatment of C2C12 cells for 24 h with 20 μM **17** or 0.1% DMSO, and CCK8 assays were performed after treatment for 24 h or 48 h with 20 μM **17** or 0.1% DMSO. (B) Phase-contrast images were obtained after treatment of HDF cells for 24 h with 20 μM **17** or 0.1% DMSO, and CCK8 assays were performed after treatment for 24 h or 48 h with 20 μM **17** or 0.1% DMSO.

Cell viability assay revealed that **17** displayed moderate cytostatic properties against human cancer cell lines: HeLa, HepG2, HT1080, MCF-7, and SK-N-MC with IC_{50} = 15.1, 16.65, 17.18, 17.58, and 17.06 μM, respectively. We also checked the status of cancer cells treated with **17** by CCK-8 assay at 24 h, 48 h and 72 h (see the Supporting Information, Figure S2). Almost all cells had vacuoles in the cytosol at 24 h, while cell viability was up to ~74.24% in HeLa cells. Therefore, HeLa cells were chosen for further analysis due to their better response to **17** treatment. Colony formation assay showed that **17** significantly reduced the colony numbers of HeLa cells in a concentration-dependent manner (see the Supporting Information, Figure S3), suggesting that exposure to **17** significantly reduced long-term cell survival.

An annexin V/PI staining was performed to investigate whether its toxicity was related to the induction of apoptosis in HeLa cells. Significant increase of the number of apoptotic and necrotic cells was observed in cells exposure to **17** in a time- and dose-dependent manner (see the Supporting Information, Figure S4). To further determine whether caspase pathway is involved in **17**-induced cell death, caspase-3 and PARP cleavage were analyzed by immunoblot analysis. Treatment of cells with the indicated concentrations of **17** and taxol (as a positive control) resulted in an increased cleavage of both caspase-3 and PARP1 (see the Supporting Information, Figure S5).

Our follow-up studies tried to figure out whether the loss of cell viability induced by **17** was caspase-dependent or not. HeLa cells were pre-treated with Z-VAD-FMK, a pan-caspase inhibitor for 1 h prior to **17** treatment and cell viability was assessed after 48 h incubation. It was observed that increases in cell death induced by taxol could be reversed by Z-VAD-FMK pretreatment. However, Z-VAD-FMK could not prevent cell death and vacuolization induced by **17** (Figure 3). These findings indicated that activation of caspase pathway might be a compensatory stress response rather than a cell death mechanism under such condition, which also indicated that the mechanism of **17**-induced cell death was non-apoptotic and caspase-independent. We then began to investigate whether **17** induces cell death through other non-apoptotic types of cell death pathways, such as paraptosis, neroptosis, oncosis and autophagic death. Among them, cleavage of caspase only happens in autophagic death in special cases.[6, 24, 25] We therefore examined the activation of LC3, an autophagosome marker.[26] Western blot analysis showed both the LC3-I (18 KDa) form and active, autophagosome membrane-bound LC3-II (16 KDa) form (Figure 4A). The effect of **17** on cell death was also observed in the presence of the autophagy inhibitor, 3-MA, which blocks autophagy by inhibiting the class III PI3K.[27] Western blot analysis showed that 3-MA attenuated **17**-induced LC3-II accumulation (Figure 4B), but 3-MA could not rescue **17**-induced cytotoxicity and cell vacuolization in HeLa cells (Figure 4C, D). Therefore, the autophagosome marker, LC3-II, is not essential for the formation of vacuolization in HeLa cells induced by **17**, and autophagy may be involved in **17**-induced cell death, but it was not indispensable. Taken together, these data suggest that the tumor-suppressive effects of **17** were not mediated via the induction of paraptosis and autophagy.

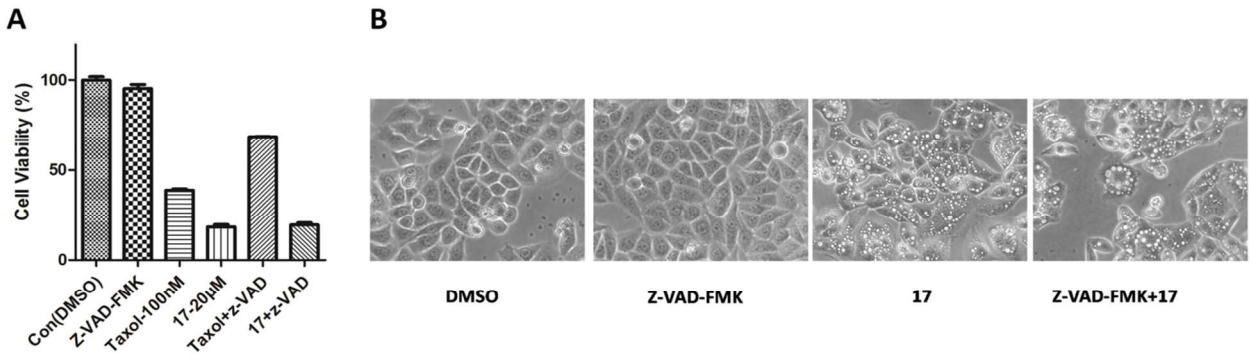

Figure 3. (A) Cell viability of HeLa cells with or without z-VAD-FMK. HeLa cells were treated with 50 μM of z-VAD-FMK for 1 h before **17** or taxol treatment. After 48 h, the cell viability was determined by CCK8 assay. (B) HeLa cells were pretreated for 1 h in the presence or absence of z-VAD-FMK prior to addition of 20 μM **17** or DMSO. Phase-contrast images were taken after 24 h.

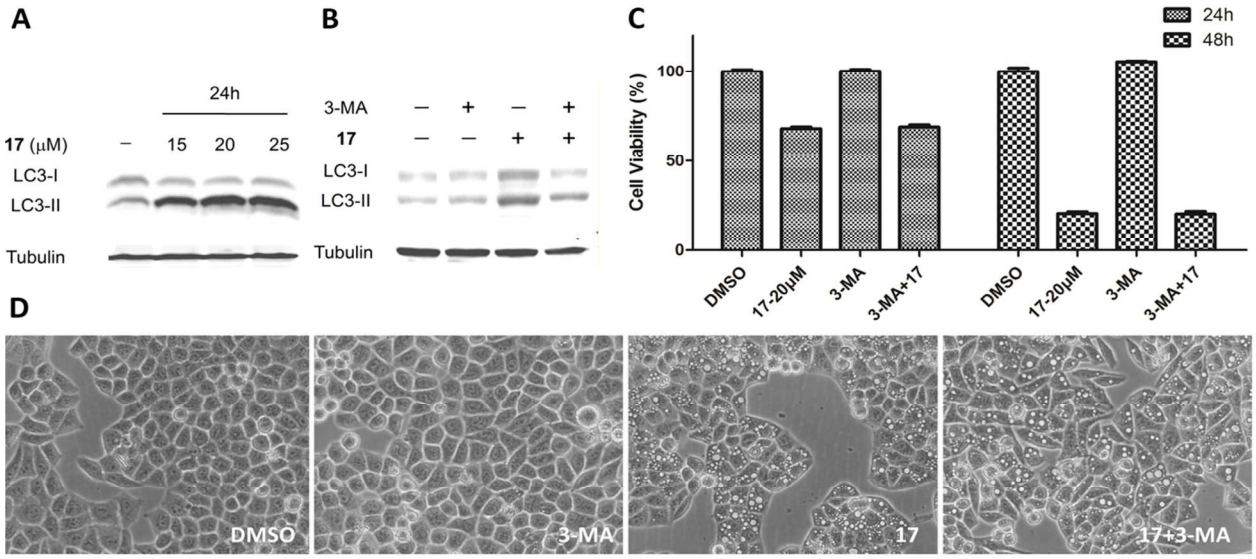

Figure 4. (A) Western blot analysis of LC3 in HeLa cells after incubation with 0.1% DMSO control or indicated concentrations of **17** for 24 h. (B) HeLa cells were pretreated for 1 h in the presence or absence of 3-MA prior to addition of **17** or DMSO. Western blot analysis of LC3

was performed after addition of 20 μM **17** for 24 h. (C) HeLa cells were pretreated for 1 h in the presence or absence of 3-MA prior to addition of **17** or DMSO. CCK8 assays were performed after treatment for 24 h or 48 h with 20 μM **17** or 0.1% DMSO. (D) HeLa cells were pretreated for 1 h in the presence or absence of 3-MA prior to addition of **17** or DMSO. Phase-contrast images were obtained after treatment of cells for 24 h.

Notably, HeLa cells exhibit clear cytoplasmic vacuolization during **17**-induced cell death. To identify the origin of the **17**-induced vacuoles and detect subtle changes in organelle ultra structure, HeLa cells were treated with **17** for 24 h and studied by transmission electron microscopy, in which cytosolic vacuolization was clearly visible. **17**-treated HeLa cells did not display the apoptotic or autophagic ultrastructural characteristics, like pyknotic chromatin or cytosolic autophagosomes (Figure 5A). Numerous electron-lucent vacuoles ranging from 0.5-2 μm in diameter were generally devoid of cytoplasmic components or organelles. Some larger vacuoles about 5 μm in diameter were distinct from autophagosomes, which have luminal cytoplasmic contents surrounded by double layers of membranes. The morphological characteristics of the dying cells did not fit the descriptions of apoptosis and autophagic cell death, and were more similar to the morphological characteristics which were previously observed in cells undergoing macropinocytosis.

The formation of large vacuoles is one of the most important characters of macropinocytosis. In order to monitor the progress of vacuole formation induced by **17**, time lapse phase-contrast microscopy was performed.[28] Live-cell imaging at 10x magnification covering the period from directly before to 72 hours after **17** treatment revealed the formation of vacuoles within 4 hours of **17** treatment in HeLa cells (see the Supporting Information, Movie S1). As has been shown,

more and more vacuoles formed in the cytoplasm and then merged with each other to form large vacuoles, finally resulting in membrane rupture and cell death (Figure 5B).

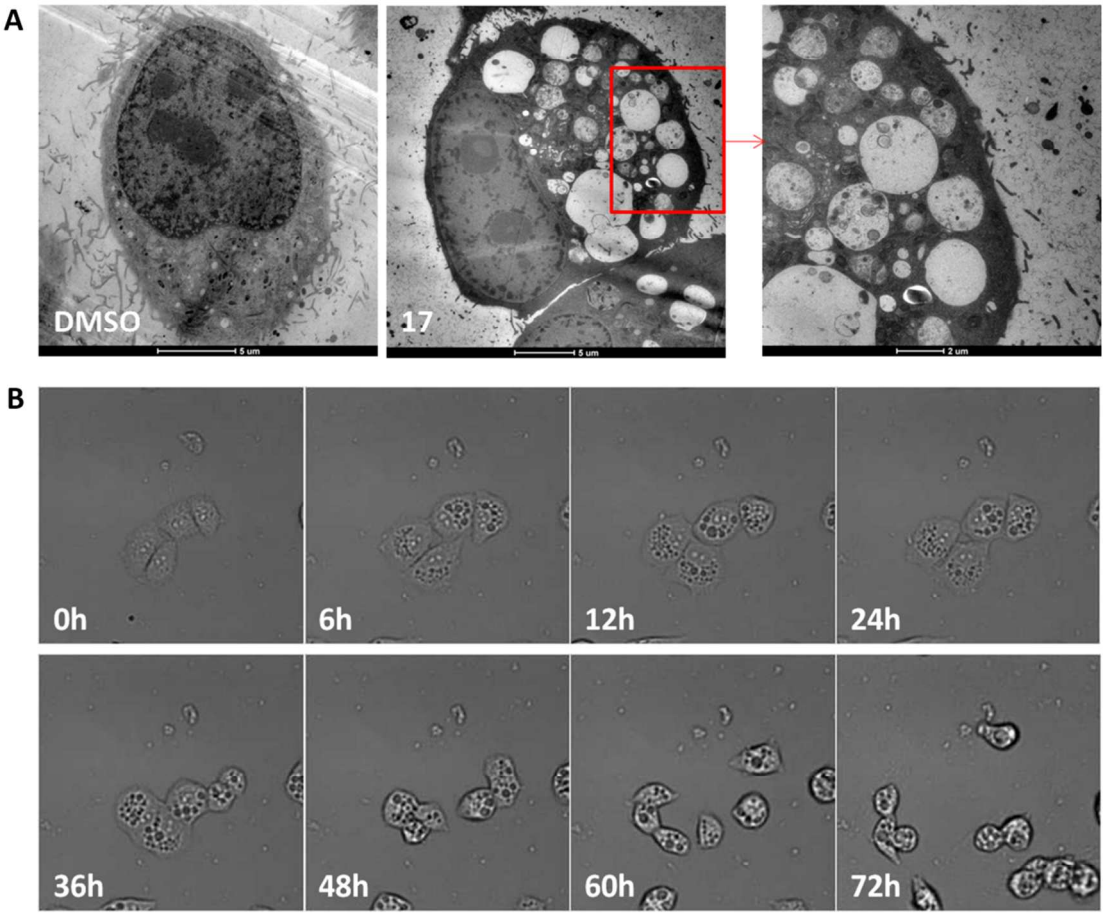

Figure 5. 17 induced cell death via a macropinocytosis-like vacuolization. (A) TEM examination of morphology changes of HeLa cells with or without 20 μM **17** for 24 h. (B) Time-lapse phase-contrast microscopy of HeLa cells treated with **17**. Images were captured at 90 sec intervals after the addition of **17** at 20 μM.

As we consider possible molecular mechanisms that **17** causes cell death through macropinocytosis, our attention was drawn to a series of studies that have defined the signaling pathway related to macropinocytosis.[29] One of the typical features of macropinocytosis is the

incorporation of extracellular-phase fluid tracers.[30] Lucifer Yellow (LY) is a well-established tracer of fluid-phase pinocytosis that is impermeable to cellular membranes.[31] Live cell imaging showed that LY was accumulated in the phase-lucent vacuoles induced by **17**, similar to what was observed with macropinocytosis in previous studies (Figure 6A). [10, 24, 28, 32] The distribution of the mitochondrial marker MitoTracker red and LysoTracker red were measured in HeLa cells after treatment with **17** (20 μM) for 24 h to further confirm the origin of the vacuoles. Live Cell Imaging with fluorescent tracers demonstrated HeLa cells contained lysosomal or mitochondrial degradative compartments, but most vacuoles induced by **17** in HeLa cells showed little overlap with these trackers (Figure 6A). To further determine whether the ability of **17** to induce cell vacuolization is correlated with macropinocytosis, we performed immunofluorescence assay to examine the colocalization of LY and the early endosomal marker EEA1, the late endosomal marker Rab7 and the late endosomal and lysosomal marker LAMP-1.[28, 33, 34] EEA1 represented a transition state between nascent and mature macropinosomes. As shown in Figure 6B, LY had minimal fusion with EEA1. Immunofluorescence analysis demonstrated that LY in HeLa cells exposed to **17** displayed an increased fusion with Rab7 and LAMP-1 with time, macropinosomes acquired characteristics of late endosomes and ultimately fused with lysosomes, which was consistent with these previous studies on macropinosomes.[35, 36]

These results are consistent with what were observed about macropinocytosis in methuosis and the concept that the vacuoles are not derived from swollen mitochondria or lysosomes, [8, 37] but ultimately macropinosomes have fusion with lysosomes, which makes the vacuoles acquire some characteristics of lysosomes. These results suggest that the vacuolization in HeLa cells induced by **17** is associated with macropinocytosis.

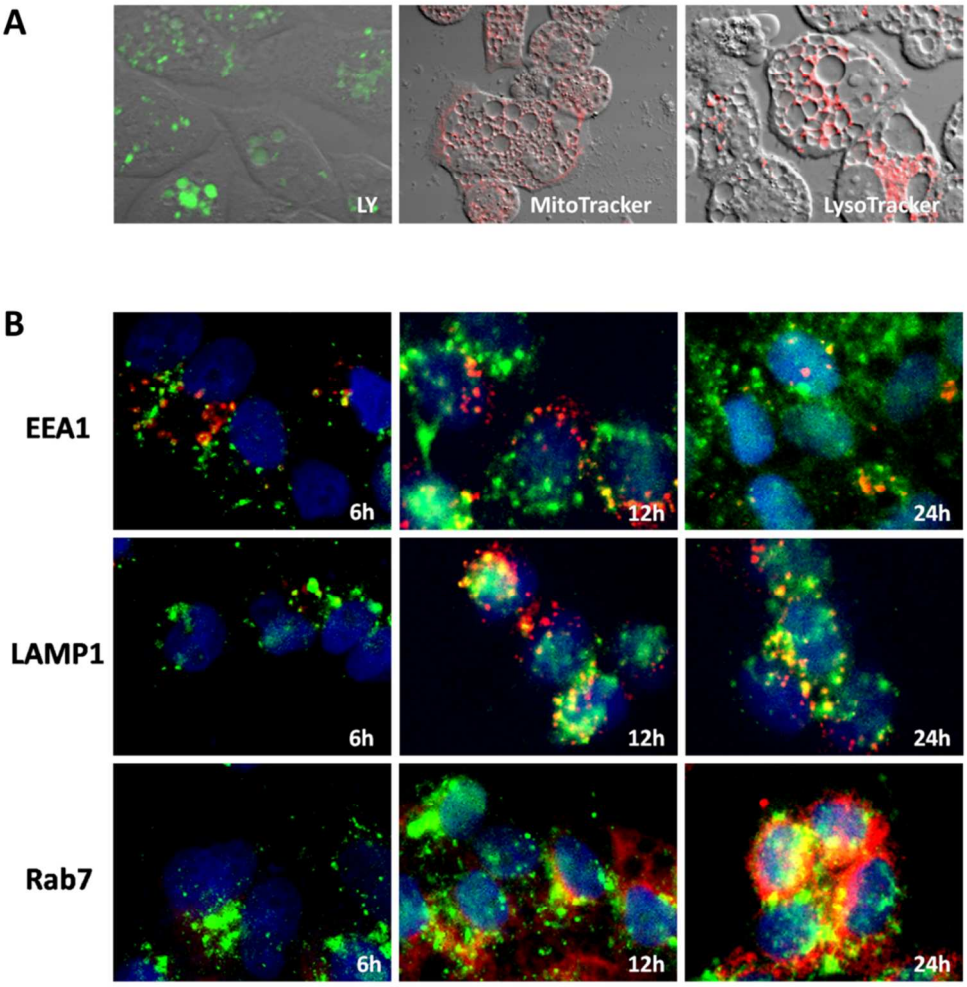

Figure 6. 17 induces macropinocytosis with cytoplasmic vacuolization. (A) Confocal microscopic analysis of LY accumulation, lysosome and mitochondria in HeLa cells. After being treated with 20 μM **17** for 24 h, cells were incubated with Lucifer yellow CH (1.25 mg/ml in HBSS) for 20 min at 37 °C, or followed by labeling with 50 nM LysoTracker Red or 200 nM MitoTracker Red CMXRos. Phase contrast and fluorescent images of the living cells were obtained using a LSM710 confocal microscope. (B) HeLa cells were treated with 0.1% DMSO control or 20 μM **17** for the indicated time, and incubated with Lucifer yellow CH followed by

staining with anti-EEA1, anti-LAMP1, anti-Rab7 and DAPI. Images were acquired on a LSM710 confocal microscope.

Methuosis is a novel form of cell death depending on the hyperstimulation of macropinocytosis. The hyperstimulation of macropinocytosis leads to membrane ruffling, formation of randomly sized vacuoles and rupture of cell.[24] Based on these findings, we test if macropinocytosis is an essential progress in **17**-induced cell death. To explore the possible contribution of macropinocytosis to **17**-induced extensive cytoplasmic vacuolization and cell death, we utilized the specific inhibitor of the vacuolar-type H^+-ATPase, Bafilomycin A1 (Baf-A), which could block clathrin-independent endocytosis, like macropinocytosis.[9] Incubation of HeLa cells with 100 nM Baf-A1 for 1 h prior to **17** treatment mitigated the formation of vacuoles, and significantly inhibited the cytotoxicity of **17** (see the Supporting Information, Figure S6 and S7). Macropinocytosis is an actin-dependent process, which also requires dynamin to mediate the release of endocytic vesicles.[38] Actin mediates membrane ruffling and leads to the formation of macropinosomes, which is a characteristic of macropinocytosis distinguishing it from other forms of endocytosis.[39] When the dynamin inhibitor and actin inhibitor, Dynasore and Cytochalasin-D,[40, 41] were added before **17** treatment, there was little diminution of cell vacuolization, but cell viability was blocked (see the Supporting Information, Figure S6 and S7).

To further explore the macropinocytosis in cell death induced by **17**, we pre-treated HeLa cells with amiloride (EIPA), a specific inhibitor of macropinocytosis through inhibiting the Na^+/H^+ ion exchange to affect the intracellular pH. We examined macropinocytic activity by counting the number of HeLa cells with macropinososomes. EIPA could significantly inhibit vacuolization of HeLa cells induced by **17** (Figure 7A), and the cell death induced by **17** was significantly blocked by EIPA (Figure 7B). These results demonstrate that the cell death induced

by **17** is macropinocytosis-dependent, and macropinocytic activity of HeLa cells under EIPA pre-treatment decrease with cell proliferation.

These data suggested macropinocytosis played an important role in **17**-induced cell death. Compound **17** was toxic to cancer cells, while EIPA could attenuate **17**-induced cell death by inhibiting macropinocytosis. Taken together with the previous studies of these inhibitors, our results supported the idea that the mechanism of **17**-induced cell death was the perturbations of endocytic trafficking that led to cellular vacuolization associated with macropinocytosis, as was the case for methuosis.

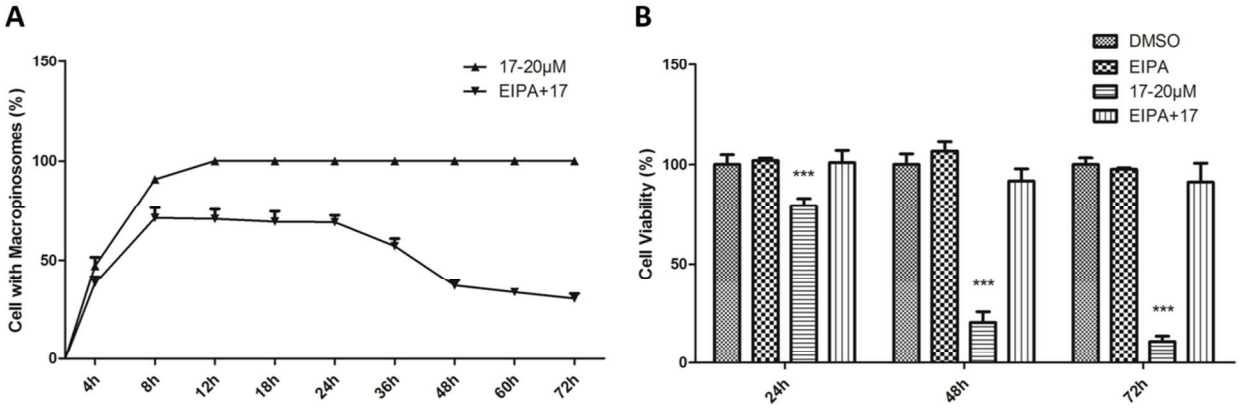

Figure 7. 17 triggers methuosis through hyperstimulation of macropinocytosis. (A) HeLa cells were pretreated for 30 min in the presence or absence of 50 μM EIPA prior to addition of 20 μM **17** or DMSO at the indicated time. At each time point, digital images of cells with macropinosomes in a field were scored manually for assessing the rate of macropinocytosis. Macropinosome quantification was performed by calculating the percentage of cells with macropinosomes. (B) HeLa cells were pretreated for 30 min in the presence or absence of 50 μM EIPA prior to addition of 20 μM **17** or DMSO. CCK8 assay was performed at the indicated time.

Drug resistance phenotypes decrease the clinical efficacy of anticancer therapies.[42] Apoptosis, taken as a caspase-dependent cell death, is the most common and recognized form of

programmed cell death. Inhibition of apoptosis is a major type of drug resistance, which is usually caused by some gene mutations.[43] Various forms of non-apoptotic cell death have been defined in the fields of toxicology and cancer therapy by different cell death phenotype, including paraptosis, autophagic death, necrosis, methuosis and so on.[24,44] Among these cell death subroutines, methuosis as a novel form of cell death is characterized by an abnormal or dysregulated macropinocytosis.[8,45] In this study, we examined the impact of **17** on macropinocytosis and the relationship between macropinocytosis and methuosis, a novel non-apoptotic cell death induced by **17**.

CONCLUSIONS

In summary, we described compound **17**, a natural-product-derived small molecule, was a novel inducer of macropinocytosis, ultimately leading to cell death. **17** provided an attractive molecular probe for studying the potential link between macropinocytosis and cell death. Our results also demonstrated, for the first time, that **17** triggered methuosis, an unusual form of non-apoptotic cell death through trafficking macropinosomes that eventually acquired some characteristics of late endosomes and lysosomes, resulting in catastrophic vacuolization and rupture of cell membrane in cancer cells. Future research will be focused on elucidating the exact targets and process of **17** in methuosis. **17** may serve as a prototype for new drugs that could be used to induce non-apoptotic death in cancer. Activation of macropinocytosis is largely pH-dependent and cancer cells are more acidic than normal cells,[46] which may provide a clue as to why cancer cells are more sensitive to **17** treatment. More insights into this unconventional form of cell death would offer new and exciting therapeutic opportunities for cancers.

EXPERIMENTAL SECTION

General Procedures. All reagents were purchased from commercial suppliers and were used directly without further purification. Flash chromatography was carried out with silica gel (200-300 mesh). Analytical TLC was performed with silica gel GF254 plates, and the products were visualized by UV detection. ^{1}H and ^{13}C NMR (500 MHz and 125 MHz, respectively) spectra were recorded in $CDCl_3$, CD_3OD or DMSO-d^6 at room temperature. The chemical shifts (δ) are provided in ppm using TMS as internal standard, and the coupling constants (*J*) are given in Hz. The following abbreviations for multiplicities are used: s, singlet; d, doublet; dd, double doublet; t, triplet; q, quadruplet; m, multiplet; and br, broad. HRMS spectra were recorded on Agilent Techologies 6230 TOF LC/MS spectrometer. Purify of compounds for biological testing was confirmed to be >95% as determined by HPLC analysis (for data, see Supporting Information). HPLC analysis was conducted according to the following method with the retention time expressed in min at UV detection of 210 nm. For HPLC method, an Agilent 1260 series HPLC instrument was used, with chromatography performed on a ZORBAX 100 mm × 4.6 mm, 3.5 μM C18 column with mobile phase gradient of 50-100% CH_3CN in H_2O with a flow rate of 1.0 mL/min.

*Benzyl (1S,2R,4aS,6aS,6bR,8aR,10S,12aR,12bR,14bS)-10-hydroxy-1,2,6a,6b,9,9,12a-heptamethyl-1,3,4,5,6,6a,6b,7,8,8a,9,10,11,12,12a,12b,13,14b-octadecahydro-picene-4a(2H)-carboxylate (**2**).* A mixture of ursolic acid **1** (460 mg, 1.0 mmol), K_2CO_3 (280 mg, 2.0 mmol) in *N,N*-dimethylformamide (10 mL) was treated with BnBr (300 mg, 1.7 mmol). The reaction mixture was heated at 60 ^{o}C for 4 h. After cooling, the mixture was poured into 50 mL of water and white solid was appeared, which was filtered, washed with H_2O and dried under vacuum to give the title compound **2** (0.50 g, 92%) as a white solid. ^{1}H NMR (500 MHz, $CDCl_3$): δ= 7.36-7.29 (m, 5H), 5.24-5.23 (m, 1H), 5.10 (d, *J* = 12.5 Hz, 1H), 4.98 (d, *J* = 12.5 Hz, 1H), 3.20 (dd, *J*

= 11.0, 4.5 Hz, 1H), 2.04-1.98 (m, 1H), 1.89-1.76 (m, 3H), 1.73-1.67 (m, 2H), 1.64-1.55 (m, 4H), 1.53-1.44 (m, 6H), 1.37-1.26 (m, 6H), 1.07 (s, 3H), 1.05-1.02 (m, 2H), 0.98 (s, 3H), 0.93 (d, *J* = 6.0 Hz, 3H), 0.89 (s, 3H), 0.85 (d, *J* = 6.5 Hz, 3H), 0.78 (s, 3H), 0.64 (s, 3H) ppm. ^{13}C NMR (125 MHz, $CDCl_3$): δ= 177.3, 138.1, 136.3, 128.4 (2C), 128.1 (2C), 127.9, 125.7, 79.0, 66.0, 55.2, 52.9, 48.1, 47.5, 42.0, 39.5, 39.1, 38.8, 38.7, 38.6, 36.9, 36.6, 33.0, 30.6, 28.1, 27.9, 27.2, 24.2, 23.5, 23.2, 21.2, 18.3, 17.0 (2C), 15.6, 15.4.

*Benzyl (1S,2R,4aS,6aS,6bR,8aR,12aR,12bR,14bS)-1,2,6a,6b,9,9,12a-heptamethyl-10-oxo-1,3,4,5,6,6a,6b,7,8,8a,9,10,11,12,12a,12b,13,14b-octadeca-hydropicene-4a(2H)-carboxylate (**3**).* To a cooled solution of compound **2** (450 mg, 0.82 mmol) in anhydrous CH_2Cl_2 (50 mL) was added PCC (355 g, 1.6 mmol). The reaction mixture was then stirred at room temperature for 12 h. Upon completion, the reaction mixture was filtered through a pad of celite. The filtrate was evaporated under reduced pressure and the residue was subjected to silica gel column chromatography to afford the title compound **3** (375 mg, 84%) as a white solid. ^{1}H NMR (500 MHz, $CDCl_3$): δ = 7.37-7.29 (m, 5H), 5.25 (t, *J* = 3.5 Hz, 1H), 5.11 (d, *J* = 12.5 Hz, 1H), 4.99 (d, *J* = 12.5 Hz, 1H), 2.57-2.50 (m, 1H), 2.40-2.34 (m, 1H), 2.27 (d, *J* = 11.5 Hz, 1H), 2.04-1.98 (m, 1H), 1.92-1.87 (m, 3H), 1.82-1.68 (m, 3H), 1.64-1.54 (m, 3H), 1.50-1.41 (m, 5H), 1.35-1.28 (m, 4H), 1.10-1.07 (m, 1H), 1.08 (s, 6H), 1.03 (d, *J* = 9.0 Hz, 6H), 0.93 (d, *J* = 6.0 Hz, 3H), 0.85 (d, *J* = 6.5 Hz, 3H), 0.68 (s, 3H) ppm. ^{13}C NMR (125 MHz, $CDCl_3$): δ= 177.2, 138.2, 136.3, 128.4 (2C), 128.1 (2C), 127.9, 125.4, 66.0, 55.2, 52.9, 48.1, 47.4, 46.7, 42.1, 39.4, 39.3, 39.1, 38.8, 36.6, 36.5, 34.2, 32.5, 30.6, 27.9, 26.5, 24.2, 23.5, 23.3, 21.4, 21.1, 19.5, 17.0, 16.9, 15.2.

Selected Experimental Procedure. *Benzyl (1S,2R,4aS,6aS,6bR,8aR,12aR,12bR,14bS)-11-formyl-1,2,6a,6b,9,9, 12a-heptamethyl-10-oxo-,3,4,5,6,6a,6b,7,8,8a,9,10,11,12,12a,12b,13,14b-*

*octadecahydropicene-4a(2H)-carboxylate (**4**, R^1 = H).* A mixture of compound **3** (300 mg, 0.55 mmol, 1.0 equiv) in anhydrous THF (20 mL) was treated with sodium methoxide (45 mg, 0.83 mmol, 1.5 equiv) at 0 ^oC, followed by the addition of ethyl formate (45 mg, 0.60 mmol, 1.1 equiv). After being stirred at room temperature for 4 h, the reaction was quenched by the addition of H_2O, and the mixture was extracted with EtOAc (3 x 30 mL). The combined organic layers were washed with brine, dried over Na_2SO_4, and concentrated to give a crude product, which was used directly in the next step without further purification. Analytical samples could be obtained by silica gel column chromatography. ^{1}H NMR (500 MHz, $CDCl_3$): δ = 14.92 (br s, 1H), 8.57 (s, 1H), 7.37-7.30 (m, 5H), 5.28 (t, J = 3.3 Hz, 1H), 5.12 (d, J = 12.5 Hz, 1H), 4.99 (d, J = 12.5, 1H), 2.32-2.28 (m, 2H), 2.05-1.92 (m, 4H), 1.82-1.69 (m, 3H), 1.65-1.56 (m, 2H), 1.50-1.43 (m, 3H), 1.39-1.26 (m, 5H), 1.18 (s, 3H), 1.14-1.10 (m, 2H), 1.11 (s, 3H), 1.08 (s, 3H), 0.94 (d, J = 6.5 Hz, 3H), 0.89 (s, 3H), 0.86 (d, J = 6.5 Hz, 3H), 0.68 (s, 3H) ppm. ^{13}C NMR (125 MHz, $CDCl_3$): δ= 177.2, 138.1, 136.3, 128.4 (2C), 128.2 (2C), 127.9, 125.4, 105.8, 66.0, 53.0, 52.0, 48.1, 45.5, 42.2, 40.1, 39.4, 39.3, 39.1, 38.8, 36.6, 36.2, 32.3, 30.6, 28.4, 27.9, 24.2, 23.4, 23.3, 21.1, 20.9, 19.4, 17.0, 16.9, 14.6. HRMS (ESI): *m/z* $[M+H]^+$ calcd for $C_{38}H_{52}O_4$: 572.3866; found: 572.3871.

Selected Experimental Procedure. *Benzyl (1S,2R,4aS,6aS,6bR, 8aR,13aR,13bR,15bS)-10-(4-cyanophenyl)-1,2,6a,6b,9,9,13a-heptamethyl-1,2,3,4,5,6,6a,6b,7,8,8a,9,10,13,13a,13b,14,15b-octadecahydro-4aH-chryseno[1,2-f]indazole-4a-carboxylate (**5**, R^1 = H, R^2 = 4-cyanophenyl).* A mixture of **4** (320 mg, 560 mmol, 1.0 equiv), 4-cyanophenylhydrazine hydrochloride (95 mg, 560 mmol, 1.0 equiv) in ethanol (20 mL) was refluxed at 85 °C for 12 h. After cooling the reaction to room temperature, the solvents were removed and the residue was partitioned between ethyl acetate and water (20 mL). The organic layer was separated and evaporated. The

residue was purified by silica gel column chromatography to afford compound **5** (315 mg, 84%) as a pale solid. ^{1}H NMR (500 MHz, $CDCl_3$): δ = 7.78 (d, *J* = 8.5 Hz, 2H), 7.55 (d, *J* = 8.5 Hz, 2H), 7.34 (s, 1H), 7.37-7.31 (m, 5H), 5.32 (t, *J* = 3.0 Hz, 1H), 5.12 (d, *J* = 12.5, 1H), 4.98 (d, *J* = 12.5 Hz, 1H), 4.14-4.09 (m, 1H), 2.77 (d, *J* = 15.5 Hz, 1H), 2.31 (d, *J* = 11.0 Hz, 1H), 2.15 (d, *J* = 15.5 Hz, 1H), 2.05-1.99 (m, 3H), 1.90-1.84 (m, 1H), 1.82-1.60 (m, 4H), 1.50-1.47 (m, 3H), 1.39-1.24 (m, 6H), 1.12-1.08 (m, 1H), 1.09 (s, 3H), 1.03 (s, 3H), 1.02 (s, 3H), 0.95 (s, 3H), 0.93 (s, 3H), 0.88 (d, *J* = 3.9 Hz, 3H), 0.69 (s, 3H) ppm. ^{13}C NMR (125 MHz, $CDCl_3$): δ = 177.3, 146.7, 146.5, 139.5, 138.1, 136.4, 132.6, 130.0, 128.5 (2C), 128.2 (2C), 128.0, 125.7, 118.1, 115.1, 112.9, 66.1, 58.5, 54.6, 53.1, 48.3, 46.4, 42.2, 39.5, 39.2, 38.9, 38.0, 37.1, 36.7, 34.7, 32.6, 30.7, 29.7, 28.0, 24.3, 23.4, 23.3, 22.8, 21.2, 19.2, 18.5, 17.0, 16.9, 15.5. HRMS (ESI): *m/z* $[M+H]^+$ calcd for $C_{45}H_{55}N_3O_2$: 669.4294; found: 669.4283.

Selected Experimental Procedure. *(1S,2R,4aS,6aS,6bR,8aR,13aR,13bR,15bS)-10-(4-Cyanophenyl)-1,2,6a,6b,9,9,13a-heptamethyl-1,2,3,4,5,6,6a,6b,7,8,8a,9,10,13,13a,3b,14,15b-octadecahydro-4aH-chryseno[1,2-f]indazole-4a-carboxylic acid (**17**).* A mixture of benzyl ester **5** (67 mg, 0.1 mmol), 10% Pd/C (10 mg) in methanol (20 mL) was stirred under 1 atm H_2 at room temperature and the reaction process was monitored by TLC. After completion of the reaction, the mixture was filtered through a pad of celite and washed with CH_3OH (10 mL). The filtrate was evaporated to dryness, and the residue was triturated with ethyl ether (2 x 10 mL). The solid was collected and dried in vacuum to give **17** as a white solid (48 mg, 82%). ^{1}H NMR (500 MHz, $CDCl_3$): δ = 10.95 (br s, 1H), 7.75 (d, *J* = 8.5 Hz, 2H), 7.52 (d, *J* = 8.5 Hz, 2H), 7.37 (s, 1H), 5.32 (t, *J* = 3.5 Hz, 1H), 2.64 (d, *J* = 15.0 Hz, 1H), 2.23 (d, *J* = 11.5 Hz, 1H), 2.14 (d, *J* = 15.5 Hz, 1H), 2.05-1.99 (m, 3H), 1.90-1.84 (m, 1H), 1.72-1.66 (m, 4H), 1.53-1.49 (m, 3H), 1.42-1.26 (m, 6H), 1.15-1.12 (m, 1H), 1.10 (s, 3H), 1.03 (s, 3H), 0.99 (s, 3H), 0.95 (d, *J* = 6.5 Hz,

3H), 0.93 (s, 3H), 0.89 (d, J = 6.0 Hz, 3H), 0.84 (s, 3H) ppm. ^{13}C NMR (125 MHz, $CDCl_3$): δ = 183.6, 146.6, 146.2, 139.3, 137.8, 132.5 (2C), 129.9 (2C), 125.6, 117.9, 115.0, 112.9, 54.4, 52.6, 47.9, 46.3, 42.1, 39.4, 39.1, 38.7, 37.9, 36.9, 36.6, 34.6, 32.3, 30.6, 29.5, 27.9, 24.0, 23.4, 23.2, 22.7, 21.1, 19.1, 16.9, 16.7, 15.4. HRMS (ESI): *m/z* $[M+H]^+$ calcd for $C_{44}H_{63}N_4O_2$: 579.3825; found: 579.3816.

Cell Culture. HeLa, HepG2, MCF-7, SY5Y, A549, HDFs and C2C12 cell lines were obtained from the Shanghai Institute of Cell Biology (Shanghai, China). Cells were grown at 37 ^{o}C with 5% CO_2 in Dulbecco's modified Eagle's medium (DMEM) (Gibco, Carlsbad, CA) supplemented with 10% fetal bovine serum (FBS) (Gibco, Carlsbad, CA) and 100 U/ml penicillin and 100 μg/ml streptomycin (Life Technologies, Grand Island, NY). All cell lines were maintained at 37 °C in 5% CO_2 humidified air.

Cell Viability Assay. Cell viability was detected by a Cell Counting Kit-8 (CCK-8; Dojindo, Japan) according to the manufacturer's instructions. Briefly, 5000 cells per well were seeded in a 96-well plate. Pre-incubate the plate overnight. Then cells were subjected to various conditions. 10 μL of CCK-8 solution was added into the each well. The absorbance was measured at 450 nm using a microplate reader (SPECTRAFLUOR, TECAN, Sunrise, Austria). The group treated with DMSO was regarded as control. In each experiment, six paralleled wells were made and all the experiments were independently repeated at least three times.

For IC_{50} determination, compound **17** was dissolved at 100 mM, with subsequent serial dilution in dimethyl sulfoxide (DMSO). Then cells were seeded in 96-well plate at the density of 1000 cells/well, and cultured with serial **17** (final concentration 0-50 μM) for 48 h. At the end of incubation, CCK-8 assay was performed. IC_{50} values of **17** were calculated with Prism

(GraphPad Software). Values are presented as an IC_{50} in μM with s.d. (n = 3 independent experiments)

Colony Formation Assay. HeLa cells were treated with various concentrations of **17** (15 μM, 20 μM, 25 μM) for 48 h before collection. Then cell from each group were seeded in six-well plates at a density of 500 cells per well. Colony formation was assessed after 15 days by fixing with methanol and staining with Giemsa. Colonies were photographed and counted.

Apoptosis Assay. In order to evaluate apoptosis, cells were stained using the Alexa Fluor® 488 annexin V/Dead Cell Apoptosis Kit (Invitrogen) as per the manufacturer's instructions. After incubation under various conditions, each group of cells was harvested and washed twice in cold PBS. Then 5 μL Alexa Fluor® 488 annexin V and 1 μL 100 ug/mL PI working solution were added to each 100 μL of cell suspension in 1x annexin-binding buffer. Cells were incubated at room temperature for 15 minutes followed by adding 400 μL 1x annexin-binding buffer. The apoptosis was determined using flow cytometry (FACS Calibur, BD Bioscience), and 10000 events from each sample were acquired to ensure adequate data. Unstained cells were used as gating controls.

Western Blot Analysis. Primary antibodies against caspase-3, PARP1, and LC3 were obtained from (Cell Signaling Technology, Danvers, MA, USA); GAPDH was purchased from Santa Cruz Biotechnology (Santa Cruz, CA). Secondary antibodies were purchased from Invitrogen. Cells were lysed in RIPA lysis buffer containing protease inhibitor cocktail (sigma, USA) on the ice for 30 min. Protein concentration was quantified using the BCA assay. Protein was separated by SDS-PAGE and was transferred onto polyvinylidene difluoride (PVDF) membrane. After being blocked with 5% non-fat milk for 1 h at room temperature, the membranes were incubated with primary antibodies overnight at 4 °C. Then the membranes were

washed with TBST buffer, and incubated with corresponding secondary antibodies at room temperature for 2 h. The protein bands were washed again with TBST buffer, and visualized by the Odyssey Infrared imaging system (Li-Cor Biosciences, Lincoln, NE). GAPDH was used as a loading control for normalization.

Time-Lapse Imaging. 50,000 HeLa cells were plated in a 20 mm glass bottom culture dish (NEST Biotechnology). Pre-incubate the plate overnight. Then cells were treated with **17** at 20 μM. The dish was placed in a live cell chamber with 5% CO_2 and 37 °C. Live imaging was performed using an Olympus 1 x 80 inverted microscope. Phase-contrast images were acquired every 90 sec for 72 hours.

Live Cell Imaging. Lucifer yellow CH, MitoTracker Red CMXRos and LysoTracker Red were purchased from Invitrogen/Molecular Probes (Carlsbad, CA). Lucifer yellow (LY) was a favorite tool for monitoring Extracellular fluid uptake. After being treated with compound for 24 h, cells were incubated with LY (1.25 mg/mL in HBSS) for 20 min at 37 °C and washed with PBS twice. To visualize active lysosome and mitochondria in cells, LysoTracker and MitoTracker Red CMXRos were used, respectively, according to the directions supplied by the manufacturers. Briefly, cells were incubated with 50 nM LysoTracker Red in medium for 30 min to label intracellular acidic compartments. Staining the mitochondria was performed by incubating live cells with 200 nM MitoTracker Red CMXRos in medium for 1 h. Phase contrast and fluorescent images of the living cells were obtained using a LSM710 confocal microscope (Zeiss).

Electron Microscopy. HeLa cells were exposed to 20 μM **17** for 24 h, and then fixed, dehydrated, embedded in resin. Images were obtained by the Electron Microscopy Facility at National Center for Protein Science Shanghai, Institute of Biochemistry and Cell Biology

(Shanghai, China). Ultrathin sections were mounted on copper grids, and then stained with uranyl acetate and lead citrate. TEM was performed with a FEI Tecnai G2 Spirit Twin electron microscope (FEI Co., Eindhoven, The Netherlands).

Immunofluorescence Analysis. Following treatment of HeLa cells on poly-L-lysine-coated glass coverslips, cells were fixed with 4% paraformaldehyde (PFA) for 30 min and permeablized with 0.1% Triton X-100 for 15 min at room temperature. Then, nonspecific binding sites were blocked by 5% bovine serum albumin (BSA) for at room temperature. For staining, HeLa cells were incubated with anti-LAMP-1 primary antibody at 4 °C overnight. Subsequently, cells were incubated for 1 h at room temperature with Alexa Fluor488-conjugated secondary antibody. Finally, nuclei were stained with 6-diamino-2-phenylindole dihydrochloride (DAPI) for 15 min. Images were acquired on a LSM710 confocal microscope with 488- and 405-nm laser excitation and ZEN software (Carl Zeiss, Oberkochen, Germany).

Quantitative Assessment of Macropinocytosis. The macropinocytosis quantification assay measuring the amount of cell with macropinosomes was performed as described previously.[47] HeLa cells were incubated with EIPA (50 μM) for 30 min, and then treated with **17** for 4 h, 8 h, 12 h, 18 h, 24 h, 36 h, 48 h, 60 h and 72 h, respectively. At each time point, digital images of cells with macropinosomes in a field were scored manually for assessing the rate of macropinocytosis. Macropinosome quantification was performed by calculating the percentage of cells with macropinosomes.

ASSOCIATED CONTENT

Supporting Information

The Supporting Information is available free of charge on the ACS Publication website at http://pubs.acs.org. Additional figures illustration inhibition data; vacuole formation movies; copies of NMR spectra; analytical HPLC data on tested compounds (PDF); SMILES molecular strings (CSV)

AUTHOR INFORMATION

Corresponding Author

*For W. Wei (lead contact): Phone: (+86)21-20350941; E-mail: weiwg@sari.ac.cn.

*For L. Li: Phone: (+86)21-62933629; E-mail: lil@sjtu.edu.cn.

ORCID

Wanguo Wei: 0000-0002-2429-8281

Notes

The authors declare no competing financial interest.

ACKNOWLEDGMENTS

This work was partially supported by grants from the Chinese Ministry of Science and Technology (2013CB967402), NSFC (21202100, 81502985), Science and Technology Commission of Shanghai Municipality (16140902100), and the Strategic Priority Research Program of the Chinese Academy of Sciences (XDA01040302). We thank Dr. Naitao Wang and Dr. Minglei Wang for help with Time-Lapse Imaging.

ABBREVIATIONS USED

UA, ursolic acid; DMF, *N,N*-dimethylformide; THF, tetrahydrofuran; DMSO, dimethyl sulfoxide; CCK-8, Cell Counting Kit-8; PARP, Poly[ADP-ribose] polymerase; LC3,

(microtubule-associated protein 1 light chain 3; 3-MA, 3-Methyladenine; PI3K, phosphoinositide 3-kinase; TEM, Transmission electron microscopy; LY, Lucifer Yellow; LAMP-1, Lysosomal-associated membrane protein 1; EEA1, Early Endosome Antigen 1; HBSS, Hank's Balanced Salt Solution; Baf-A, Bafilomycin A1; EIPA, amiloride; DMEM, Dulbecco's modified Eagle's medium; FBS, fetal bovine serum; PVDF, polyvinylidene difluoride; PFA, paraformaldehyde; BSA, bovine serum albumin; DAPI, 6-diamino-2-phenylindole dihydrochloride

REFERENCES

(1) Peetla, C.; Vijayaraghavalu, S.; Labhasetwar, V. Biophysics of cell membrane lipids in cancer drug resistance: Implications for drug transport and drug delivery with nanoparticles. *Adv. Drug Delivery Rev.* **2013,** *65,* 1686-1698.

(2) Gottesman, M. M. Mechanisms of cancer drug resistance. *Annu. Rev. Med.* **2002,** *53,* 615-627.

(3) Qiao, L.; Wong, B. C. Targeting apoptosis as an approach for gastrointestinal cancer therapy. *Drug Resist. Updates* **2009,** *12,* 55-64.

(4) Brosh, R.; Rotter, V. When mutants gain new powers: news from the mutant p53 field. *Nat. Rev. Cancer* **2009,** *9,* 701-713.

(5) Lo, P. K.; Sukumar, S. Epigenomics and breast cancer. *Pharmacogenomics* **2008,** *9,* 1879-1902.

(6) Lockshin, R. A.; Zakeri, Z. Apoptosis, autophagy, and more. *Int. J. Biochem. Cell Biol.* **2004,** *36,* 2405-2419.

(7) Galluzzi, L.; Vitale, I.; Abrams, J. M.; Alnemri, E. S.; Baehrecke, E. H.; Blagosklonny, M. V.; Dawson, T. M.; Dawson, V. L.; El-Deiry, W. S.; Fulda, S.; Gottlieb, E.; Green, D. R.; Hengartner, M. O.; Kepp, O.; Knight, R. A.; Kumar, S.; Lipton, S. A.; Lu, X.; Madeo, F.; Malorni, W.; Mehlen, P.; Nunez, G.; Peter, M. E.; Piacentini, M.; Rubinsztein, D. C.; Shi, Y.; Simon, H. U.; Vandenabeele, P.; White, E.; Yuan, J.; Zhivotovsky, B.; Melino, G.; Kroemer, G. Molecular definitions of cell death subroutines: recommendations of the nomenclature committee on cell death 2012. *Cell Death Differ.* **2012,** *19,* 107-120.

(8) Overmeyer, J. H.; Kaul, A.; Johnson, E. E.; Maltese, W. A. Active ras triggers death in glioblastoma cells through hyperstimulation of macropinocytosis. *Mol. Cancer Res.* **2008,** *6,* 965-977.

(9) Kaul, A.; Overmeyer, J. H.; Maltese, W. A. Activated Ras induces cytoplasmic vacuolation and non-apoptotic death in glioblastoma cells via novel effector pathways. *Cell Signaling* **2007,** *19,* 1034-1043.

(10) Overmeyer, J. H.; Young, A. M.; Bhanot, H.; Maltese, W. A. A chalcone-related small molecule that induces methuosis, a novel form of non-apoptotic cell death, in glioblastoma cells. *Mol. Cancer* **2011,** *10,* 69.

(11) Robinson, M. W.; Overmeyer, J. H.; Young, A. M.; Erhardt, P. W.; Maltese, W. A. Synthesis and evaluation of indole-based chalcones as inducers of methuosis, a novel type of nonapoptotic cell death. *J. Med. Chem.* **2012,** *55,* 1940-1956.

(12) Kalani, K.; Yadav, D. K.; Singh, A.; Khan, F.; Godbole, M. M.; Srivastava, S. K. QSAR guided semi-synthesis and in-vitro validation of anticancer activity in ursolic acid derivatives. *Curr. Top. Med. Chem.* **2014,** *14,* 1005-1013.

(13) Xiao, S.; Wang, Q.; Si, L.; Shi, Y.; Wang, H.; Yu, F.; Zhang, Y.; Li, Y.; Zheng, Y.; Zhang, C.; Wang, C.; Zhang, L.; Zhou, D. Synthesis and anti-HCV entry activity studies of beta-cyclodextrin-pentacyclic triterpene conjugates. *ChemMedChem.* **2014,** *9,* 1060-1070.

(14) Sathya, S.; Sudhagar, S.; Sarathkumar, B.; Lakshmi, B. S. EGFR inhibition by pentacyclic triterpenes exhibit cell cycle and growth arrest in breast cancer cells. *Life Sci.* **2014,** *95,* 53-62.

(15) Andersson, D.; Liu, J. J.; Nilsson, A.; Duan, R. D. Ursolic acid inhibits proliferation and stimulates apoptosis in HT29 cells following activation of alkaline sphingomyelinase. *Anticancer Res.* **2003,** *23,* 3317-3322.

(16) Tang, C.; Lu, Y. H.; Xie, J. H.; Wang, F.; Zou, J. N.; Yang, J. S.; Xing, Y. Y.; Xi, T. Downregulation of survivin and activation of caspase-3 through the PI3K/Akt pathway in ursolic acid-induced HepG2 cell apoptosis. *Anticancer Drugs* **2009,** *20,* 249-258.

(17) Chen, H.; Gao, Y.; Wang, A.; Zhou, X.; Zheng, Y.; Zhou, J. Evolution in medicinal chemistry of ursolic acid derivatives as anticancer agents. *Eur. J. Med. Chem.* **2015,** *92,* 648-655.

(18) Saraswat, B.; Visen, P. K.; Agarwal, D. P. Ursolic acid isolated from eucalyptus tereticornis protects against ethanol toxicity in isolated rat hepatocytes. *Phytother. Res.* **2000,** *14,* 163-166.

(19) Suh, N.; Honda, T.; Finlay, H. J.; Barchowsky, A.; Williams, C.; Benoit, N. E.; Xie, Q. W.; Nathan, C.; Gribble, G. W.; Sporn, M. B. Novel triterpenoids suppress inducible nitric oxide synthase (iNOS) and inducible cyclooxygenase (COX-2) in mouse macrophages. *Cancer Res.* **1998,** *58,* 717-723.

(20) Liu, M. C.; Yang, S. J.; Jin, L. H.; Hu, D. Y.; Xue, W.; Song, B. A.; Yang, S. Synthesis and cytotoxicity of novel ursolic acid derivatives containing an acyl piperazine moiety. *Eur. J. Med. Chem.* **2012,** *58,* 128-135.

(21) Rashid, S.; Dar, B. A.; Majeed, R.; Hamid, A.; Bhat, B. A. Synthesis and biological evaluation of ursolic acid-triazolyl derivatives as potential anti-cancer agents. *Eur. J. Med. Chem.* **2013,** *66,* 238-245.

(22) Vitaku, E.; Smith, D. T.; Njardarson, J. T. Analysis of the structural diversity, substitution patterns, and frequency of nitrogen heterocycles among U.S. FDA approved pharmaceuticals. *J. Med. Chem.* **2014,** *57,* 10257-10274.

(23) You, Y. J.; Kim, Y.; Nam, N. H.; Ahn, B. Z. Synthesis and cytotoxic activity of A-ring modified betulinic acid derivatives. *Bioorg. Med. Chem. Lett.* **2003,** *13,* 3137-3140.

(24) Maltese, W. A.; Overmeyer, J. H. Methuosis: nonapoptotic cell death associated with vacuolization of macropinosome and endosome compartments. *Am. J. Pathol.* **2014,** *184,* 1630-1642.

(25) Marino, G.; Niso-Santano, M.; Baehrecke, E. H.; Kroemer, G. Self-consumption: the interplay of autophagy and apoptosis. *Nat. Rev. Mol. Cell Biol.* **2014,** *15,* 81-94.

(26) Kimura, S.; Noda, T.; Yoshimori, T. Dissection of the autophagosome maturation process by a novel reporter protein, tandem fluorescent-tagged LC3. *Autophagy* **2007,** *3,* 452-460.

(27) Blommaart, E. F.; Krause, U.; Schellens, J. P.; Vreeling-Sindelarova, H.; Meijer, A. J. The phosphatidylinositol 3-kinase inhibitors wortmannin and LY294002 inhibit autophagy in isolated rat hepatocytes. *Eur. J. Biochem.* **1997,** *243,* 240-246.

(28) Kitambi, S. S.; Toledo, E. M.; Usoskin, D.; Wee, S.; Harisankar, A.; Svensson, R.; Sigmundsson, K.; Kalderen, C.; Niklasson, M.; Kundu, S.; Aranda, S.; Westermark, B.; Uhrbom, L.; Andang, M.; Damberg, P.; Nelander, S.; Arenas, E.; Artursson, P.; Walfridsson, J.; Forsberg Nilsson, K.; Hammarstrom, L. G.; Ernfors, P. Vulnerability of glioblastoma cells to catastrophic vacuolization and death induced by a small molecule. *Cell* **2014,** *157,* 313-328.

(29) Swanson, J. A. Shaping cups into phagosomes and macropinosomes. *Nat. Rev. Mol. Cell Biol.* **2008,** *9,* 639-649.

(30) Mercer, J.; Helenius, A. Gulping rather than sipping: macropinocytosis as a way of virus entry. *Curr. Opin. Microbiol.* **2012,** *15,* 490-499.

(31) Belichenko, P. V.; Dahlstrom, A. Studies on the 3-dimensional architecture of dendritic spines and varicosities in human cortex by confocal laser scanning microscopy and Lucifer yellow microinjections. *J. Neurosci. Methods* **1995,** *57,* 55-61.

(32) Cai, H.; Liu, J.; Fan, Q.; Li, X. [Methuosis: a novel type of cell death]. *Nan Fang Yi Ke Da Xue Xue Bao* **2013,** *33,* 1844-1847.

(33) Maltese, W. A.; Overmeyer, J. H. Non-apoptotic cell death associated with perturbations of macropinocytosis. *Front Physiol.* **2015,** *6,* 38.

(34) Dutta, S.; Roy, S.; Polavaram, N. S.; Stanton, M. J.; Zhang, H.; Bhola, T.; Honscheid, P.; Donohue, T. M., Jr.; Band, H.; Batra, S. K.; Muders, M. H.; Datta, K. Neuropilin-2 regulates endosome maturation and EGFR trafficking to support cancer cell pathobiology. *Cancer Res.* **2016,** *76,* 418-428.

(35) Hewlett, L. J.; Prescott, A. R.; Watts, C. The coated pit and macropinocytic pathways serve distinct endosome populations. *J. Cell Biol.* **1994,** *124,* 689-703.

(36) West, M. A.; Bretscher, M. S.; Watts, C. Distinct endocytotic pathways in epidermal growth factor-stimulated human carcinoma A431 cells. *J. Cell Biol.* **1989,** *109,* 2731-2739.

(37) Racoosin, E. L.; Swanson, J. A. Macropinosome maturation and fusion with tubular lysosomes in macrophages. *J. Cell Biol.* **1993,** *121,* 1011-1020.

(38) Soda, K.; Balkin, D. M.; Ferguson, S. M.; Paradise, S.; Milosevic, I.; Giovedi, S.; Volpicelli-Daley, L.; Tian, X.; Wu, Y.; Ma, H.; Son, S. H.; Zheng, R.; Moeckel, G.; Cremona, O.; Holzman, L. B.; De Camilli, P.; Ishibe, S. Role of dynamin, synaptojanin, and endophilin in podocyte foot processes. *J. Clin. Invest.* **2012,** *122,* 4401-4411.

(39) Kerr, M. C.; Teasdale, R. D. Defining macropinocytosis. *Traffic* **2009,** *10,* 364-371.

(40) Macia, E.; Ehrlich, M.; Massol, R.; Boucrot, E.; Brunner, C.; Kirchhausen, T. Dynasore, a cell-permeable inhibitor of dynamin. *Dev. Cell* **2006,** *10,* 839-850.

(41) Hitomi, J.; Christofferson, D. E.; Ng, A.; Yao, J.; Degterev, A.; Xavier, R. J.; Yuan, J. Identification of a molecular signaling network that regulates a cellular necrotic cell death pathway. *Cell* **2008,** *135,* 1311-1323.

(42) Pommier, Y.; Sordet, O.; Antony, S.; Hayward, R. L.; Kohn, K. W. Apoptosis defects and chemotherapy resistance: molecular interaction maps and networks. *Oncogene* **2004,** *23,* 2934-2949.

(43) Huang, J.; Ni, J.; Liu, K.; Yu, Y.; Xie, M.; Kang, R.; Vernon, P.; Cao, L.; Tang, D. HMGB1 promotes drug resistance in osteosarcoma. *Cancer Res.* **2012,** *72,* 230-238.

(44) Clarke, P. G. Developmental cell death: morphological diversity and multiple mechanisms. *Anat. Embryol.* **1990,** *181,* 195-213.

(45) Chi, S.; Kitanaka, C.; Noguchi, K.; Mochizuki, T.; Nagashima, Y.; Shirouzu, M.; Fujita, H.; Yoshida, M.; Chen, W.; Asai, A.; Himeno, M.; Yokoyama, S.; Kuchino, Y. Oncogenic Ras triggers cell suicide through the activation of a caspase-independent cell death program in human cancer cells. *Oncogene* **1999,** *18,* 2281-2290.

(46) Dhar, G.; Sen, S.; Chaudhuri, G. Acid gradient across plasma membrane can drive phosphate bond synthesis in cancer cells: acidic tumor milieu as a potential energy source. *PLoS One* **2015,** *10,* e0124070.

(47) Ard, R.; Mulatz, K.; Pomoransky, J. L.; Parks, R. J.; Trinkle-Mulcahy, L.; Bell J. C.; Gee, S. H. Regulation of macropinocytosis by diacylglycerol kinase zeta. *PLoS One* **2015,** *10,* e0144942.

Graphic for manuscript